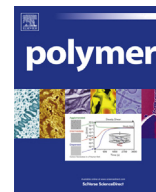




Contents lists available at ScienceDirect

Polymer

journal homepage: www.elsevier.com/locate/polymer

Polymerized ionic liquid diblock copolymers with long alkyl side-chain length

Jacob R. Nykaza, Yuesheng Ye, Yossef A. Elabd*

Department of Chemical and Biological Engineering, Drexel University, Philadelphia 19104, PA, USA

ARTICLE INFO

Article history:

Received 4 January 2014

Received in revised form

11 March 2014

Accepted 3 April 2014

Available online xxx

Keywords:

Ionic liquid

Block copolymer

Conductivity

ABSTRACT

A polymerized ionic liquid (PIL) diblock copolymer with a long alkyl side-chain, poly(MMA-*b*-MUBIm-Br), was synthesized at various compositions from an ionic liquid monomer, (1-[(2-methacryloyloxy)undecyl]-3-butylimidazolium bromide) (MUBIm-Br), and a non-ionic monomer, methyl methacrylate (MMA). The PIL diblock copolymer was synthesized *via* post-functionalization from its non-ionic precursor PIL diblock copolymer, poly(MMA-*b*-BrUMA) (BrUMA = 11-bromoundecyl methacrylate), which was synthesized *via* the reverse addition fragmentation chain transfer (RAFT) polymerization technique. Differential scanning calorimetry reveals two distinct constant glass transition temperatures (T_g s) with a low PIL segment T_g . These PIL block copolymers result in easily processable, flexible, transparent films with high mechanical strength. A high bromide ion conductivity of 64.85 mS cm^{-1} at 80°C and 90% RH was measured for the PIL diblock copolymer with an ion exchange capacity (IEC) of 1.44 meq/g (23.3 mol % MUBIm-Br). Interestingly, this result was three times higher than its analogous PIL homopolymer (2.75 meq/g ; 100 mol% MUBIm-Br) and an order of magnitude higher than a PIL block copolymer from a previous study with similar chemistry, similar IEC, higher water content, but shorter alkyl side-chain length. Ion conductivity did not scale as expected with water content, which is unusual for water-assisted ion transport (e.g., protons, hydroxide, chloride) in ion-containing polymers, and therefore suggests other mechanisms that impact ion transport in PIL block copolymers.

© 2014 Elsevier Ltd. All rights reserved.

1. Introduction

Polymerized ionic liquid (PIL) block copolymers are a distinct set of block copolymers that combine the properties of both PILs and block copolymers [1–5]. More specifically, the unique physicochemical properties of PILs include high solid-state ionic conductivity, high chemical, thermal and electrochemical stability, and widely tunable physical properties (e.g., *via* anion exchange), while block copolymers are known to self-assemble into a range of nanostructures (e.g., body-centered cubic spheres, hexagonal cylinders, bicontinuous gyroid, lamellae). In the solid-state, this self-assembly results in materials that can accelerate the transport of ions and small molecules within continuous nanostructured channels, where the PIL chemistry within these channels offer unique property advantages, such as high electrochemical stability for hydroxide or lithium ions or high preferential sorption affinity for carbon dioxide. These features have led to a recent exploration

of PIL block copolymers for a number of applications, including gas separations [6,7], electrochemical transducers [8], and fuel cells [9].

Transport in PIL block copolymers differs from other work on ion transport (conductivity)–morphology studies in block copolymers, where previous studies typically involve a mixture of either a solid salt (e.g., Li salt) or molten salt (e.g., ionic liquid (IL)) with a neutral block copolymer [10–15]. In these mixtures, the cations and anions migrate simultaneously to provide ion conduction. Contrastingly, PIL block copolymers are single-ion conductors, where one ion is covalently attached to the polymer chain (e.g., cation) and the counterion is mobile (e.g., anion). Typical counterions in PILs are fluorinated (e.g., bis(trifluoromethanesulfonyl)imide; TFSI) resulting in a hydrophobic polymer, where ion transport in the anhydrous polymer is dictated by the segmental dynamics of the polymer chains (Vogel–Fulcher–Tammann behavior with temperature) [16]. However, when these counterions are exchanged with other anions (e.g., hydroxide), the PIL becomes hydrophilic and ion transport is dictated by a water-mediated mechanism (Arrhenius behavior with temperature) [17]. Understanding how nanostructured morphology in PIL block copolymers impacts the transport of both types of ions is of

* Corresponding author.

E-mail address: elabd@drexel.edu (Y.A. Elabd).

importance for applications, such as gas separations and energy storage for the former type and fuel cells and water purification for the latter type. Recently, there have been several fundamental investigations on conductivity–morphology relationships in PIL block copolymers [1–5]. For fluorinated counterions (e.g., TFSI), morphology type [1,3], the extent of long-range order [1,4], the strength of micro-phase separation [2,3], and the glass transition temperature of the PIL microdomain [3,5] have all shown to have a significant impact on ion conductivity in PIL block copolymers.

More recently, the transport of other counterions, which are of interest for this present investigation, such as bromide and hydroxide, in PIL block copolymers has been explored, where these counterions are facilitated by a water-mediated transport mechanism. The conductivity of these counterions is of interest for alkaline exchange membrane (AEM) fuel cells and water purification applications [9]. Recent work in our laboratory [9] synthesized and investigated the bromide and hydroxide conductivity in a PIL diblock copolymer poly(MMA-*b*-MEBIm-Br) or poly(methyl methacrylate-*b*-1-[(2-methacryloyloxy)ethyl]-3-butylimidazolium bromide). In this previous work, the PIL block copolymer with 17.3 mol% MEBIm-Br composition or 1.4 meq/g ion exchange capacity (IEC) showed a high bromide conductivity of 5.67 mS cm⁻¹ at 80 °C and 90% RH. The bromide conductivity of this PIL block copolymer was over an order of magnitude higher than its analogous PIL random copolymer (at the same IEC and water content) over a temperature range of 30–80 °C at high humidity (90% RH). This was a product of the strong micro-phase separation (lamellae) in the PIL block copolymer, where no microphase separation was evident in the PIL random copolymer. Surprisingly, the bromide ion conductivity in this PIL block copolymer was higher than its analogous PIL homopolymer, which had a higher IEC (3-fold) and water content (2-fold) than the block copolymer. It is not clear why the bromide ion conductivity was higher in the block copolymer compared to the homopolymer as this has not been evidenced before in water-assisted ion transport in block copolymers to the authors' knowledge [18]. Similar conductivity trends were also observed for hydroxide ion conductivity in these PIL polymers as well, where the PIL block copolymer had a hydroxide conductivity of 25.46 mS cm⁻¹ at 80 °C and 90% RH at a low water content.

To date, there are only few reports of water-assisted ion conductivity in PIL block copolymers. However, several recent reports have investigated water-assisted ion transport in block copolymers for alkaline fuel cells [9,19–21]. Watanabe and coworkers [19] investigated hydroxide ion conductivity in aromatic multiblock copolymers of poly(arylene ether)s containing covalently attached quaternary ammonium cations. A high hydroxide ion conductivity of 144 mS cm⁻¹ at 80 °C in liquid water for the block copolymer with an IEC of 1.93 meq/g was measured, which was ~3 times higher than its analogous random copolymer at an IEC of 1.88 meq/g. The higher conductivity in the block copolymer compared to the random copolymer was attributed to a strong micro-phase separation observed in the block copolymer *via* electron microscopy. Coughlin and co-workers [20] synthesized and investigated the morphology and conductivity of the block copolymer poly(styrene-*b*-vinyl benzyl trimethylammonium hydroxide), PS-*b*-[PVBtMA][OH]. A hydroxide conductivity of 12.55 mS cm⁻¹ at 80 °C and 90% RH was measured for the block copolymer with an IEC of 1.36 meq/g. Differences in hydroxide conductivity were observed between block copolymers of varying IEC, which was attributed to differences in morphology type and d-spacing observed with small-angle X-ray scattering. Knauss and coworkers [21] synthesized bromide and hydroxide conducting poly(phenylene oxide) block and random copolymers and measured a bromide and hydroxide conductivity of 26 mS cm⁻¹ (90 °C; 95% RH) and 84 mS cm⁻¹ (80 °C; 95% RH), respectively, for the block copolymer with an IEC of

1.27 meq/g. Similar to the work of Elabd and coworkers [9], the block copolymer showed a higher conductivity compared to its analogous random copolymer.

Several of the recent observations in water-assisted ion transport in anion exchange block copolymers, such as ion conductivity higher in a block copolymer compared to its random copolymer, has previously been observed in cation exchange block copolymers (e.g., sulfonated block copolymers) [18]. However, the recent observation of ion transport higher in a block copolymer compared to its analogous homopolymer is unique and is of interest to explore further [9]. In this study, a PIL block copolymer was synthesized with a similar chemistry to a former study, poly(MMA-*b*-MEBIm-Br), however, the PIL chemistry was modified to incorporate a longer alkyl side-chain length (from C = 2 to C = 11). This should lower the glass transition temperature of the PIL domain and therefore produce more flexible films under dry conditions at room temperature. We are interested in the properties and conductivity of these new materials, particularly the conductivity of the block copolymer compared to its homopolymer.

In this paper, a PIL diblock copolymer with a long alkyl side-chain was synthesized, poly(MMA-*b*-MUBIm-Br), at various compositions comprising of a PIL component (1-[(2-methacryloyloxy)undecyl]-3-butylimidazolium bromide) (MUBIm-Br) and a non-ionic component (MMA). Poly(MMA-*b*-MUBIm-Br) was synthesized *via* post-functionalization from its non-ionic precursor PIL diblock copolymer, poly(MMA-*b*-BrUMA) (BrUMA = 11-bromoundecyl methacrylate), which was synthesized *via* the reverse addition fragmentation chain transfer (RAFT) polymerization technique. An analogous PIL homopolymer, poly(MUBIm-Br), was synthesized by conventional free radical polymerization for comparison. The thermal, mechanical, and conductivity properties of these PILs were investigated in this study.

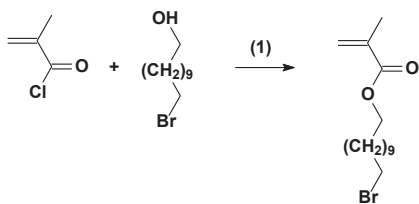
2. Experimental

2.1. Materials

4-Cyano-4-(phenylcarbonothioylthio)pentanoic acid (chain transfer agent (CTA), >97%, HPLC), tetrahydrofuran (THF, ≥99.9%), *N,N*-dimethylformamide (DMF, 99.9%, HPLC), methanol (99.9%, HPLC), acetonitrile (anhydrous, 99.8%), calcium hydride (CaH₂, 95%), lithium bromide (LiBr, ≥99%), 11-bromo-1-undecanol (98%), 1-butylimidazole (98%), magnesium sulfate (anhydrous, ReagentPlus®, 99%), triethylamine (≥99.5%), methacryloyl chloride (97%, stabilized with 200 ppm monomethyl ether hydroquinone (MEHQ)), dichloromethane (ACS reagent, ≥99.5%, contains 50 ppm amylene stabilizer), dimethyl sulfoxide-*d*₆ (DMSO-*d*₆, 99.9% atom % D, contains 0.03% v/v TMS) and chloroform-*d* (CDCl₃, 99.96 atom % D, contains 0.03% v/v TMS) were used as received from Sigma–Aldrich. Azobisisobutyronitrile (AIBN, 98%, Sigma–Aldrich) was purified by recrystallization twice from methanol. Methyl methacrylate (MMA, 99%, Sigma–Aldrich) was purified by distillation over CaH₂ at a reduced pressure. Ultrapure deionized (DI) water with resistivity ca. 16 MΩ cm was used as appropriate.

2.2. Synthesis of 11-bromoundecyl methacrylate monomer

A typical synthesis method for the bromine terminated monomer, 11-bromoundecyl methacrylate (BrUMA), which has been synthesized in a previous publication [22], is shown in Scheme 1(1) and includes adding 37.4 g (148.89 mmol) of 11-bromo-1-undecanol and 80 mL of dichloromethane to a three-neck 500 mL flask in an ice bath. Under nitrogen, a mixture of 15.24 g (150.61 mmol) of triethylamine and 40 mL of dichloromethane was slowly added to the flask, followed by a slow addition of a mixture of 15.75 g



^a(1) triethylamine, dichloromethane, room temperature, 18 h.

Scheme 1. Synthesis of 11-bromoundecyl methacrylate (BrUMA) monomer.^a

(150.67 mmol) of methacryloyl chloride and 30 mL of dichloromethane using an addition funnel. The reaction mixture was stirred at room temperature for 18 h and then was filtered. The liquid filtrate was washed with 250 mL DI water four times. The water layer was removed using a separation funnel and the residual water in the organic layer was removed with anhydrous magnesium sulfate. The organic solvent was removed by vacuum, which yielded a clear liquid of 11-bromoundecyl methacrylate (BrUMA). Yield: 23.33 g (51%). ¹H NMR (500 MHz, CDCl₃, 23 °C) δ (ppm): 6.02–6.00 (s, 1H, HCH=C(CH₃)), 5.67–5.64 (s, 1H, HCH=C(CH₃)), 4.1–4.05 (t, 2H, O–CH₂–), 3.53–3.49 (t, 2H, –CH₂–Br), 1.89–1.86 (s, 3H, CH₂=C(CH₃)), 1.8–1.75 (m, 2H, O–CH₂–CH₂–), 1.64–1.56 (m, 2H, –CH₂–CH₂–Br), 1.4–1.22 (m, 14H, O–CH₂–CH₂–(CH₂)₇–CH₂–CH₂–Br).

2.3. Synthesis of PMMA macro-CTA

The preparation of PMMA macro-chain transfer agent (macro-CTA) is shown in [Scheme 2](#)(1). 25.88 g of MMA (258.49 mmol), 142.2 mg of CTA (0.509 mmol), 21.4 mg of AIBN (0.130 mmol) were mixed with 8.5 mL THF in a 250 mL single-neck Schlenk flask. The flask was subjected to three freeze–pump–thaw degassing cycles followed by sealing the reactor and carrying out the reaction under static vacuum at 70 °C for 5 h. The resulting polymer was twice precipitated in methanol and dried under vacuum in an oven at room temperature for 24 h. Yield: 9.07 g of solid particles (35.15%). ¹H NMR (500 MHz, CDCl₃, 23 °C) δ (ppm): 7.92–7.32 (m, C₆H₅) 3.60 (s, 3H, O–CH₃), 2.0–1.76 (d, 2H, CH₂–C(CH₃)), 1.2–0.8 (d, 3H, CH₂–C(CH₃)); M_n = 19.8 kg mol^{–1} (NMR). SEC (THF, 40 °C): M_n = 19.3 kg mol^{–1}, M_w/M_n = 1.17 (against PS standards).

2.4. Synthesis of precursor diblock copolymer poly(MMA-*b*-BrUMA)

The synthesis of the non-ionic precursor block copolymer poly(MMA-*b*-BrUMA) is shown in [Scheme 2](#)(2). A typical example is

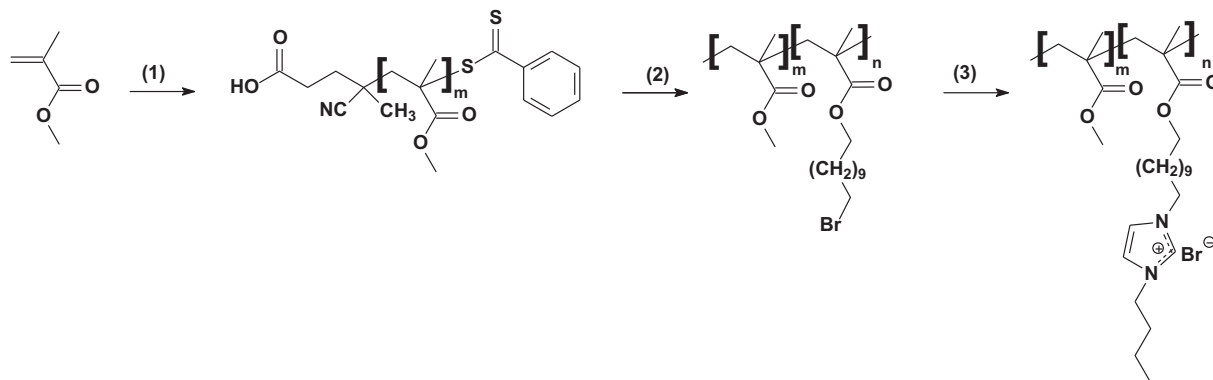
given as follows. 1.0 g (0.052 mmol) of PMMA macro-CTA in THF (PMMA/THF 1/5 w/w) was added to a 50 mL Schlenk flask. Then a mixture of 2.43 g (7.61 mmol) of 11-bromoundecyl methacrylate (BrUMA) in THF (BrUMA/THF 1/1 w/w) and 2.09 mg (0.013 mmol) AIBN were added to the flask and subjected to three freeze–pump–thaw degassing cycles. After degassing, the reactor was sealed and the reaction was carried out under vacuum at 70 °C for 6 h. The resulting polymer was twice precipitated in methanol. The block copolymer was filtered and then dried under vacuum in an oven at room temperature for 24 h. Yield: 1.78 g (51.9%). ¹H NMR (500 MHz, CDCl₃, 23 °C) δ (ppm): 4.0–3.9 (s, 2H, O–CH₂–CH₂–), 3.7 (s, 3H, O–CH₃), 3.56–3.38 (t, 2H, –CH₂–CH₂–Br), 2.0–1.70 (d, 2H, CH₂–C(CH₃)), 1.65–1.52 (2H, m, O–CH₂–CH₂–), 1.45–1.30 (2H, s, –CH₂–CH₂–Br), 1.35–1.2 (m, 14H, O–CH₂–CH₂–(CH₂)₇–CH₂–CH₂–Br), 1.00–0.77 (3H, m, CH₂–C(CH₃)); M_n = 34.5 kg mol^{–1} (NMR). SEC (THF, 40 °C): M_n = 28.4 kg mol^{–1}, M_w/M_n = 1.48 (against PS standards).

2.5. Synthesis of PIL diblock copolymer poly(MMA-*b*-MUBIm-Br)

The synthesis of the ionic PIL block copolymer (poly(MMA-*b*-MUBIm-Br-23.3)) is shown in [Scheme 2](#)(3), i.e., functionalization of non-ionic precursor block copolymer to form ionic PIL block copolymer. A typical example is given as follows. 0.99 g (0.029 mmol) of poly(MMA-*b*-BrUMA) in DMF (poly(MMA-*b*-BrUMA)/DMF = 1/2 w/w) and 0.933 g (7.51 mmol) of 1-butylimidazole (BrUMA/1-butylimidazole 1/3 mol/mol) were added to a 50 mL vial and reacted at 70 °C for 72 h. The resulting polymer was precipitated into hexane three times and dried under vacuum in an oven at room temperature for 24 h. Yield: 1.77 g of solid particles (91.6%). ¹H NMR (500 MHz, DMSO-*d*₆, 23 °C) δ (ppm) 9.68 (s, 1H, N–CH=N), 8.0–7.7 (d, 2H, N–CH=CH–N), 4.3–4.2 (d, 4H, N–CH₂–CH₂–CH₂–), 4.0–3.9 (t, 2H, O–CH₂–CH₂–), 3.7 (s, 3H, O–CH₃), 1.88 (s, 4H, CH₂–C(CH₃), N–CH₂–CH₂–CH₂–CH₃), 1.52 (m, 2H, O–CH₂–CH₂–), 1.3–1.1 (m, 18H, O–CH₂–CH₂–(CH₂)₈–, N–CH₂–CH₂–CH₂–CH₃), 1–0.85 (s, 6H, N–CH₂–CH₂–CH₂–CH₃, CH₂–C(CH₃)), 0.75 (s, 3H, CH₂–C(CH₃)). M_n = 41.5 kg mol^{–1} (NMR).

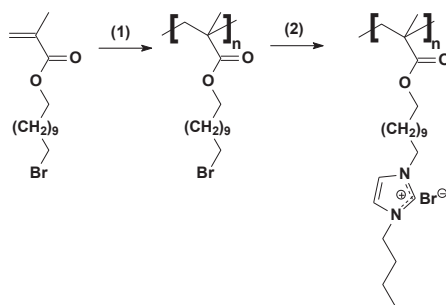
2.6. Synthesis of precursor homopolymer poly(BrUMA)

The synthesis of the non-ionic precursor homopolymer, poly(-BrUMA), was performed using conventional free-radical polymerization as shown in [Scheme 3](#)(1). A typical example is given as follows. 4.0 g (12.57 mmol) of BrUMA monomer in DMF (BrUMA/DMF 1/2 w/w) and 10.4 mg (0.064 mmol) AIBN were mixed in a 200 mL round bottom flask and reacted under N₂ for 3.5 h at 65 °C.



^a(1) 4-cyano-4-(phenylcarbonothioylthio)pentanoic acid (CTA), AIBN, THF, 70 °C, 5 h; (2) BrUMA, AIBN, THF, 70 °C, 6 h; (3) 1-butylimidazole, DMF, 70 °C, 72 h.

Scheme 2. Synthesis of poly(MMA-*b*-MUBIm-Br) block copolymers.^a



^a(1) AIBN, DMF, 65 °C, 3.5 h; (2) 1-butylimidazole, DMF, chloroform, 70 °C, 72 h.

Scheme 3. Synthesis of poly(MUBIm-Br) homopolymer.^a

The resulting polymer was precipitated into methanol twice and dried under vacuum in an oven at room temperature for 24 h. Yield: 0.62 g of solid particle (15.5%). ¹H NMR (500 MHz, CDCl₃, 23 °C) δ (ppm): 3.9–3.8 (s, 2H, O–CH₂–CH₂–), 3.5–3.3 (m, 2H, –CH₂–CH₂–Br), 1.85–1.75 (d, 2H, CH₂–C(CH₃)), 1.60–1.47 (2H, m, O–CH₂–CH₂–), 1.40–1.32 (2H, s, –CH₂–CH₂–Br), 1.32–1.1 (m, 14H, O–CH₂–CH₂–(CH₂)₇–CH₂–CH₂–Br), 0.95–0.75 (3H, m, CH₂–C(CH₃)). SEC (THF, 40 °C): $M_n = 43.23 \text{ kg mol}^{-1}$, $M_w/M_n = 4.28$ (against PS standards).

2.7. Synthesis of PIL homopolymer poly(MUBIm-Br)

The synthesis of the ionic PIL homopolymer, poly(MUBIm-Br), is shown in Scheme 3(2), i.e., functionalization of non-ionic precursor homopolymer to form ionic PIL homopolymer. A typical example is given as follows. 0.5258 g (0.012 mmol) of poly(BrUMA) was first dissolved in 1 mL chloroform in a 50 mL vial. 0.614 g (4.94 mmol) 1-butylimidazole (poly(BrUMA)/1-butylimidazole, 1/3 mol/mol) along with 2 mL DMF were then mixed into the vial. The solution was reacted at 70 °C for 72 h. The resulting polymer was precipitated into hexane three times and dried under vacuum in an oven at room temperature for 24 h. Yield: 0.452 g of solid particles (63.2%). ¹H NMR (500 MHz, DMSO-*d*₆, 23 °C) δ (ppm): 9.75–9.6 (s, 1H, N–CH=N), 8.05–7.75 (d, 2H, N–CH=CH–N), 4.3–4.15 (d, 4H, N–CH₂–CH₂–CH₂–), 4.0–3.9 (t, 2H O–CH₂–CH₂–), 1.85–1.75 (s, 4H, CH₂–C(CH₃), N–CH₂–CH₂–CH₂–CH₃), 1.55–1.45 (m, 2H, O–CH₂–CH₂–), 1.3–1.1 (m, 18H, O–CH₂–CH₂–(CH₂)₈–, N–CH₂–CH₂–CH₂–CH₃), 0.9–0.85 (s, 3H, N–CH₂–CH₂–CH₂–CH₃), 0.75 (s, 3H, CH₂–C(CH₃)).

2.8. Solvent-casting PIL block copolymer and homopolymer films

PIL block copolymer, poly(MMA-*b*-MUBIm-Br), films were fabricated by first dissolving the polymer in anhydrous acetonitrile (10% w/w) and subsequently casting onto Teflon substrates (ca. 35 mm (*L*) × 4 mm (*W*) × 0.525 mm (*T*)) under ambient conditions for 24 h. The polymer films were subsequently annealed under vacuum at 150 °C for 72 h. PIL homopolymer, poly(MUBIm-Br), films were fabricated by dissolving the polymer in anhydrous acetonitrile (12.5% w/w) and casting on glass substrates under ambient conditions for 24 h followed by annealing under vacuum at room temperature for 72 h. These annealed films were used to characterize physical properties. The film thickness, ranging between 100 and 200 μm , were measured with a Mitutoyo digital micrometer with $\pm 0.001 \text{ mm}$ accuracy.

2.9. Characterization

All chemical structures, PIL compositions, and number-average molecular weights were characterized by ¹H NMR spectroscopy

using a Varian 500 MHz spectrometer at 23 °C with either CDCl₃ or DMSO-*d*₆ as the solvent. The chemical shifts were referenced to tetramethylsilane (TMS). The molecular weights and molecular weight distributions of PMMA macro-CTA, non-ionic precursor block copolymers, and non-ionic precursor homopolymer were determined by size exclusion chromatography (SEC) using a Waters GPC system equipped with a THF Styragel column (Styragel@HR⁵E, effective separation of molecular weight range: 2–4000 kg mol^{−1}) and a 2414 reflective index (RI) detector. All measurements were performed at 40 °C. THF was used as the mobile phase at a flow rate of 1.0 mL/min. PS standards (Shodex, Japan) with molecular weights ranging from 2.97 to 591 kg mol^{−1} were used for calibration. Glass transition temperatures (*T*_gs) were determined by differential scanning calorimetry (DSC; TA Instruments, Q200) over a temperature range of −100 to 150 °C at a heating/cooling rate of 10 °C/min under a N₂ environment using a heat/cool/heat method. *T*_g was determined using the midpoint method from the second thermogram heating cycle.

The ionic (bromide) conductivities of the polymer films were measured with electrochemical impedance spectroscopy (EIS, Solartron, 1260 impedance analyzer, 1287 electrochemical interface, Zplot software) over a frequency range of 1 Hz–10⁷ Hz at 300 mV. Conductivities were collected under humidified conditions, where temperature and relative humidity were controlled by an environmental chamber (Tenney, BTRS model). The in-plane conductivities of the PIL films were measured in a cell with four-parallel electrodes, where an alternating current was applied to the outer electrodes and the real impedance or resistance, *R*, was measured between the two inner reference electrodes. The resistance was determined from a high *x*-intercept of the semi-circle regression of the Nyquist plot. Conductivity was calculated by using the following equation: $\sigma = l/AR$, where *l* and *A* are the distance between two inner electrodes and the cross section area of the polymer film ($A = Wl$; *W* is the film width and *l* is the film thickness), respectively. Samples were allowed to equilibrate for 1 h at each temperature and humidity followed by six measurements, one every 10 min, at the equilibrium condition. The values reported are an average of these steady-state measurements. An average error of <5% was observed between these multiple steady-state values and duplicate experiments. For conductivity measurements in liquid water, polymer films were immersed in DI water for 1 h and then placed in the four-electrode cell. Liquid water was added to the cell and on top of the film to maintain full hydration throughout the experiment. Six steady state scans were performed and the average of these was reported.

Water uptake or content was measured with dynamic vapor sorption (DVS, TA Instruments Q5000). A dry sample was first loaded into the DVS and preconditioned at 0% RH and 30 °C for 2 h to remove any residual water in the sample. Only a small weight

loss (<0.5%) was observed during this 2 h period and the loss in mass did not change well before the end of this 2 h time period. The temperature was systematically changed to a constant value at a fixed humidity and the film was allowed to equilibrate for 2 h at each condition. There was no change in mass prior to the end of this 2 h equilibration period indicating that equilibrium water sorption was reached. The polymer water content [wt%; g H₂O/g dry polymer × 100] was calculated as follows:

$$W_{\text{H}_2\text{O}} = \frac{W - W_0}{W_0} \times 100\% \quad (1)$$

where W_0 and W are the dry and wet polymer weights measured before and after the DVS experiment, respectively.

Mechanical properties (stress–strain behavior) of the polymer films were measured using a Kato KES G1 mechanical tensile tester. Stress–strain curves were acquired using the KES G1 with the C load cell in place and the sensitivity set to 0.2 kg/V with the 10× multiplier set for sensitivity and the crosshead speed set to 0.084 cm/s. The Kato KES G1 outputs data in voltage. Conversion from voltage to engineering stress was achieved *via* the following equations:

$$F = ma = (S)(V)(g) \quad (2)$$

$$\sigma = \frac{F}{A} \quad (3)$$

where F is the force [N], S is sensitivity [0.2 kg/V], V is the output voltage, g is acceleration due to gravity [9.8 m s⁻²], σ is the engineering stress [MPa], and A is the cross-sectional area of the film tested [m²]. Sample strain was calculated using:

$$\varepsilon = \frac{l_f - l_0}{l_0} \times 100\% \quad (4)$$

where ε is the engineering strain, l_f is the final length, and l_0 is the original length. The Young's (elastic) modulus was found using only the elastic regime of the output data and is calculated using as follows:

$$E = \frac{\sigma}{\varepsilon} \quad (5)$$

where E is the Young's modulus [MPa] and σ and ε are the stress and strain in the elastic regime, respectively. The sample sizes for this experiment were 3.0 mm × 15 mm × 0.1 mm and the samples were prepared using the same procedure as that for samples used in the conductivity experiments. A small amount of epoxy (Loctite 0.85-ounce plastic syringe epoxy quick set) was applied to the film ends to improve gripping of the sample in the C load cell. A minimum of three samples were tested to ensure repeatability and the average and standard deviation of these repeated experiments were reported.

3. Results and discussion

3.1. Synthesis and chemical characterization

We synthesized a series of polymerized ionic liquid (PIL) diblock copolymers (poly(MMA-*b*-MUBIm-Br)) with long alkyl side-chain length ($C = 11$) at various MUBIm-Br (or PIL) compositions and its analogous PIL homopolymer (poly(MUBIm-Br)). Non-ionic precursor PIL block copolymers and PIL homopolymer were first synthesized *via* reversible addition-fragmentation chain transfer (RAFT) polymerization and conventional free-radical

polymerization, respectively. The non-ionic precursor block copolymers and homopolymer were subsequently post-functionalized to form ionic PIL block copolymers and PIL homopolymer.

The synthesis of the precursor IL monomer, (11-BrUMA), is shown in Scheme 1(1). The chemical structure was confirmed by ¹H NMR and is shown in Fig. 1. The precursor IL monomer was polymerized by conventional free radical polymerization to form the precursor PIL homopolymer, poly(BrUMA), as shown in Scheme 3(1). ¹H NMR was used to confirm that no unreacted monomer remained in the polymer from the disappearance of the double bond peaks at 6.01 and 5.68 ppm that were evidenced in the monomer. The reaction conditions and molecular weight of poly(-BrUMA) are listed in Table 1. The non-ionic precursor PIL homopolymer was then subjected to a post-functionalization reaction to covalently attach the imidazolium cation onto the bromine terminated alkyl chain to form a PIL homopolymer with a bromide anion (Br), poly(MUBIm-Br), as shown in Scheme 3(2). Complete functionalization of the PIL homopolymer was confirmed and calculated by ¹H NMR as shown in Fig. 1 by relative integrations of resonance "f" versus resonance "h" (i.e., $f1/(f1 + h/4)$) (see Table 2).

The synthesis of PIL block copolymers first consisted of polymerizing precursor block copolymers (poly(MMA-*b*-BrUMA)) at various BrUMA compositions *via* living/controlled polymerization (RAFT) (Scheme 2 (2)). The BrUMA composition was characterized by ¹H NMR as shown in Fig. 1. The non-ionic precursor block copolymers were then converted to charged PIL block copolymers (poly(MMA-*b*-MUBIm-Br)) *via* post-functionalization reaction (Scheme 2 (3)). ¹H NMR was used to determine complete functionalization of the block copolymers as shown in Fig. 1. Block copolymer compositions were calculated from relative integrations of resonance "l" versus resonance "i" (i.e., $l1/(l1 + i/3)$).

Typical SEC results for the precursor PIL homopolymer, PMMA macro-CTA, and precursor PIL block copolymer (at 23.3 mol% BrUMA) are shown in Fig. 2. Molecular weights and polydispersity determined from SEC for precursor PIL block copolymers at all BrUMA compositions are listed in Table 1. Fig. 2 clearly indicates an increase of molecular weight from the PMMA macro-CTA ($M_n = 19.3 \text{ kg mol}^{-1}$) to the precursor PIL block copolymer (poly(MMA-*b*-BrUMA-23.3), 23.3 mol% BrUMA, $M_n = 28.43 \text{ kg mol}^{-1}$). The M_n of PMMA macro-CTA measured by SEC is in good agreement with the result calculated from ¹H NMR ($M_n = 19.8 \text{ kg mol}^{-1}$, Fig. 1). The molecular weight of the precursor PIL homopolymer was higher than the PIL block copolymers ($M_n = 43.27 \text{ kg mol}^{-1}$) and the polydispersity was higher ($M_w/M_n = 4.28$) due to the use of conventional free radical polymerization. A series of precursor PIL block copolymers were synthesized with BrUMA compositions ranging from 5.4 to 37.9 mol%. The compositions and reaction conditions are listed in Table 1.

3.2. Thermal properties

Fig. 3 shows glass transition temperatures (T_g s) of the non-ionic precursor PIL block copolymers and the ionic PIL block copolymers as a function of BrUMA and MUBIm-Br compositions, respectively. Both sets were compared to a PMMA homopolymer control (0 mol% BrUMA or MUBIm-Br) and to their respective precursor PIL or PIL homopolymer controls (100 mol% BrUMA and MUBIm-Br, respectively). Note that the PMMA homopolymer control was synthesized by RAFT polymerization (i.e., PMMA macro-CTA), while the precursor PIL and PIL homopolymers were synthesized by free radical polymerization. Two distinct T_g s that do not change with composition are expected for strongly micro-phase-separated block copolymers. Fig. 3a shows that the T_g s for both the PMMA and precursor PIL homopolymers (poly(BrUMA)) are 124 °C and -48 °C,

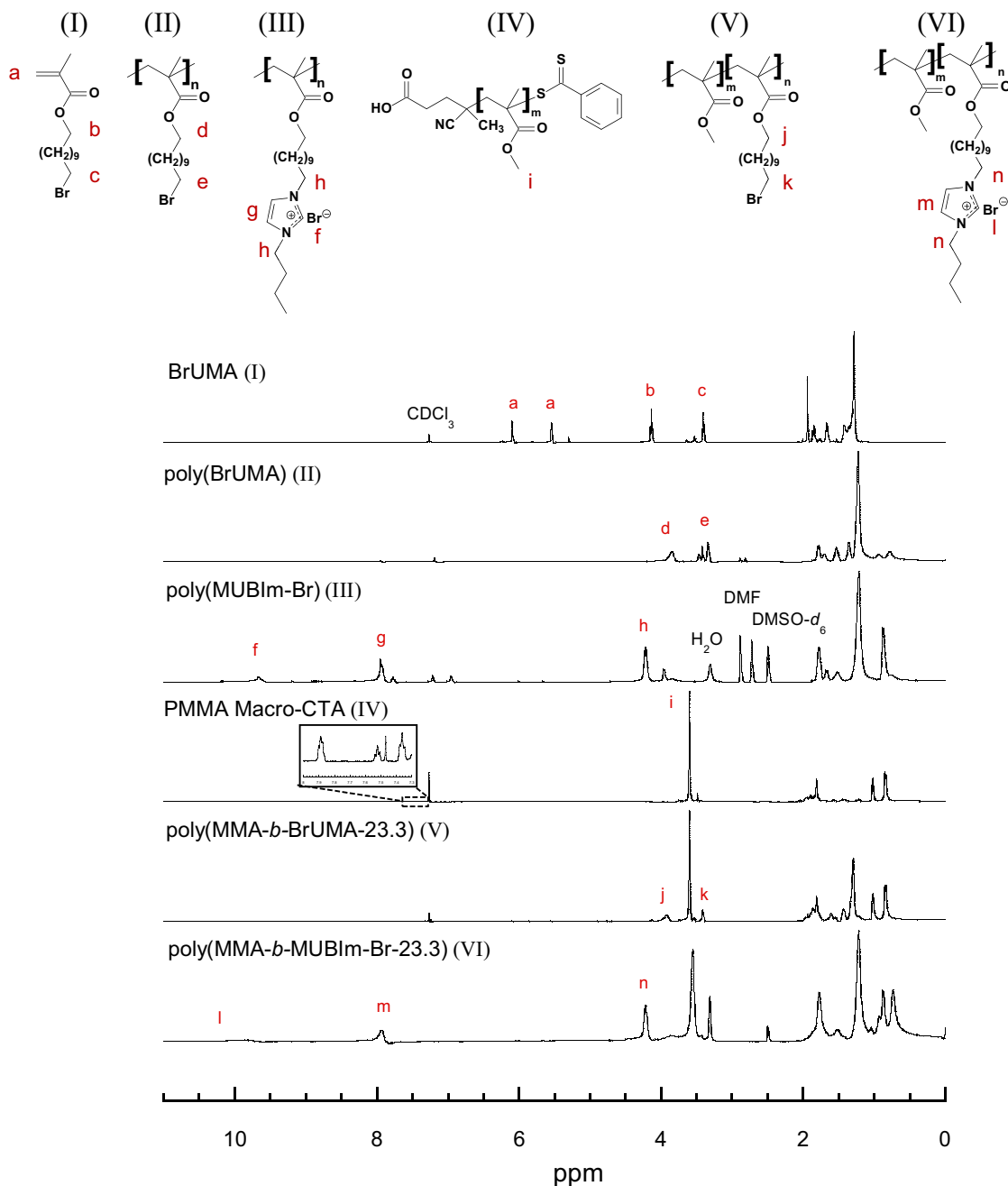


Fig. 1. ^1H NMR spectra of BrUMA (I), precursor homopolymer (poly(BrUMA)) (II), PIL homopolymer (poly(MUBIm-Br)) (III), PMMA Macro-CTA (IV), precursor block copolymer (poly(MMA-*b*-BrUMA-23.3)) (V), and PIL block copolymer (poly(MMA-*b*-MUBIm-Br-23.3)) (VI). Precursor polymers and BrUMA monomer in CDCl_3 and PIL polymers in $\text{DMSO-}d_6$. 23.3 corresponds to mol% of BrUMA and MUBIm-Br.

respectively. The precursor PIL block copolymers show two distinct constant T_g s that are similar to the homopolymer T_g s over the BrUMA composition range of 12.3–37.9 mol%. Only one glass transition was observed for the block copolymer at 5.4 mol% BrUMA composition, which may be due to the relatively low BrUMA composition.

Fig. 3b shows that the T_g s for both the PMMA and PIL homopolymers (poly(MUBIm-Br)) are 124 °C and –14 °C, respectively. Notice that the post-functionalization of the precursor PIL homopolymer to form the PIL homopolymer (attachment of the imidazolium cation) raises the T_g from –48 °C to –14 °C. Similar to the non-ionic precursor PIL block copolymers in Fig. 3a, the ionic PIL

block copolymers in Fig. 3b show two distinct T_g s over the MUBIm-Br composition range of 12.3–37.9 mol%. However, although the MMA segment in the PIL block copolymers have a similar T_g compared to the PMMA homopolymer, the T_g of the PIL segment in the PIL block copolymers are consistently higher compared to the PIL homopolymer by approximately 40 °C. This was unexpected, but may be the result of differences in chain dynamics regarding ionic interactions within the micro-domain compared to the homopolymer, which results in an even further elevation of the T_g .

The comparison between Fig. 3a and b shows that functionalization of the homopolymer to covalently attach the imidazolium cation results in an elevation of T_g from –45 °C to –14 °C. This T_g

Table 1

Reaction conditions, molecular weight of non-ionic precursor block copolymers and homopolymer.

Precursor block copolymers and homopolymer ^a	mol%	Recipe ^b	M_n (kg mol ⁻¹) ^c	M_n (kg mol ⁻¹) ^d	PDI ^d
poly(MMA- <i>b</i> -BrUMA-5.4)	5.4	10:1:0.1	19.8 + 3.4	22.52	1.19
poly(MMA- <i>b</i> -BrUMA-12.3)	12.3	35:1:0.1	19.8 + 7.76	26.45	1.26
poly(MMA- <i>b</i> -BrUMA-17.3)	17.3	50:1:0.1	19.8 + 10.9	27.51	1.33
poly(MMA- <i>b</i> -BrUMA-20.3)	20.3	60:1:0.1	19.8 + 12.8	30.42	1.38
poly(MMA- <i>b</i> -BrUMA-23.3)	23.3	100:1:0.1	19.8 + 14.7	28.43	1.48
poly(MMA- <i>b</i> -BrUMA-37.9)	37.9	150:1:0.1	19.8 + 23.9	31.26	1.46
poly(BrUMA)	100	20:0:0.1	–	43.27	4.28

^a *b* = block copolymer, numbers correspond to BrUMA mol%, which was determined from ¹H NMR spectroscopy.^b A:B:C = BrUMA:PMMA-CTA:AIBN (in mol).^c Calculated from ¹H NMR spectroscopy.^d Determined by SEC.

elevation is the result of introducing ionic groups, where it is known that electrostatic interactions among covalently attached ionic moieties results in increasing the T_g in ionomers [23]. Interestingly, the PIL segment of the PIL block copolymer elevates the T_g even further from -14 °C to ~ 24 °C when comparing to the PIL homopolymer. A shift in T_g from the homopolymer to the block copolymer sometimes indicates a weak micro-phase separation, however, this is usually indicated by both T_g s deviating from their respective homopolymer T_g s and also these two T_g s changing with composition. In Fig. 3b, only the PIL segment T_g in the PIL block copolymer deviates from the PIL homopolymer T_g and it remains constant over the entire composition range investigated. This deviation suggests another mechanism. We hypothesize that the polymer chain dynamics associated with electrostatic interactions within the PIL micro-domains differ compared to the homopolymer. Previous work in our laboratory reported on a PIL block copolymer with similar chemistry, poly(MMA-*b*-MEBIm-Br), where the primary difference to the block copolymer in this study was the alkyl side-chain length between the backbone and the imidazolium cation ($C = 2$ in previous work compared to $C = 11$ in this work) [9]. The T_g of the PIL segment of poly(MMA-*b*-MEBIm-Br) in this previous work was reported as 103 °C compared to 24 °C for poly(MMA-*b*-MUBIm-Br) reported in this work. Clearly, increasing the alkyl side-chain length results in an approximate 75–80 °C depression in the PIL segment T_g . This depression in the PIL segment T_g in the PIL block copolymer may have benefits to conductivity and mechanical properties.

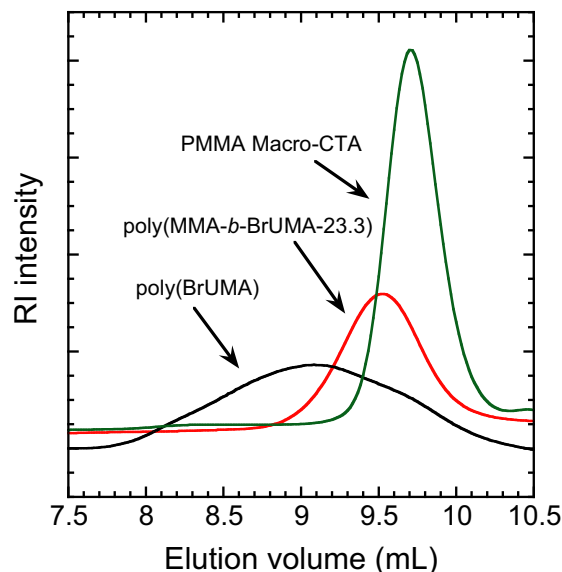
3.3. Mechanical properties

The PIL block copolymers were solution cast into free-standing films for mechanical property analysis, where Fig. 4 shows both

Table 2

PIL block copolymers and homopolymer.

Sample name ^a	mol%	wt.%	IEC ^b	T_g (°C) ^c
Poly(MMA- <i>b</i> -MUBIm-Br-5.4)	5.4	20.2	0.47	131
Poly(MMA- <i>b</i> -MUBIm-Br-12.3)	12.3	38.3	0.93	23, 124
Poly(MMA- <i>b</i> -MUBIm-Br-17.3)	17.3	48.1	1.19	24, 125
Poly(MMA- <i>b</i> -MUBIm-Br-20.3)	20.3	53.0	1.32	26, 127
Poly(MMA- <i>b</i> -MUBIm-Br-23.3)	23.3	57.3	1.44	27, 125
Poly(MMA- <i>b</i> -MUBIm-Br-37.9)	37.9	73.0	1.90	23, 124
Poly(MUBIm-Br) ^d	100	100	2.75	-14

^a Numbers correspond to PIL mol%, which was determined from ¹H NMR spectroscopy.^b Calculated as meq l^{m+} per g of polymer.^c Determined by midpoint method.^d PIL homopolymer.**Fig. 2.** SEC chromatograms of PMMA macro-CTA, precursor block copolymer (poly(MMA-*b*-BrUMA-23.3)), and precursor homopolymer (poly(BrUMA)).

flexible and transparent films can be produced at ambient conditions. Note that the T_g of the PIL segment is ~ 24 °C, where a further reduction in that T_g should be expected upon water sorption. An estimated 50 °C T_g reduction was calculated upon water sorption using the Flory–Fox equation.

The mechanical properties of the PIL block copolymer poly(MMA-*b*-MUBIm-Br-23.3) were tested at ambient conditions ($\sim 50\%$ RH and ~ 23 °C) and compared to Nafion 212 (the most frequently cited polymer membrane in fuel cells) and are listed in Table 3. Poly(MMA-*b*-MUBIm-Br-23.3) was chosen for the mechanical property measurements due to having the highest conductivity at 80 °C and 90% RH as discussed in the next section and will be the PIL composition of choice for future research for electrochemical applications. The PIL block copolymer results in a maximum tensile strength of 12.1 MPa, Young's modulus of 0.74 GPa, and elongation at break of 3.4%. Compared to Nafion 212, the PIL block copolymer has similar tensile strength and a three-fold higher Young's modulus and a significantly lower elongation at break. The mechanical properties measured here for Nafion 212 agree well with previous literature results. [24]

The low elongation at break is due to the relatively high composition (76.7 mol%) of glassy PMMA in the PIL block copolymer. However, the high composition of PMMA allows for a high modulus for the PIL block copolymer, which is required for electrochemical applications, such as alkaline fuel cells. Pure PMMA has an elongation of break of $<10\%$ and a Young's modulus of ~ 3 GPa [25]. This is one of the advantages of using block copolymers, where one block provides high mechanical strength (MMA), while the other provides accelerated transport properties (MUBIm-Br).

3.4. Conductivity

Fig. 5a shows bromide ion conductivity at 90% RH as a function temperature for all PIL block copolymers and PIL homopolymer. The bromide conductivity in all polymers follows an Arrhenius behavior with temperature at high humidity with activation energies decreasing with increasing IEC (i.e., MUBIm-Br composition): 96.6, 54.7, 81.1, 86.2, 39.4 kJ mol⁻¹. The PIL homopolymer exhibits the lowest activation energy of 18.2 kJ mol⁻¹. At 50 °C and 90% RH, the PIL homopolymer has the highest conductivity of

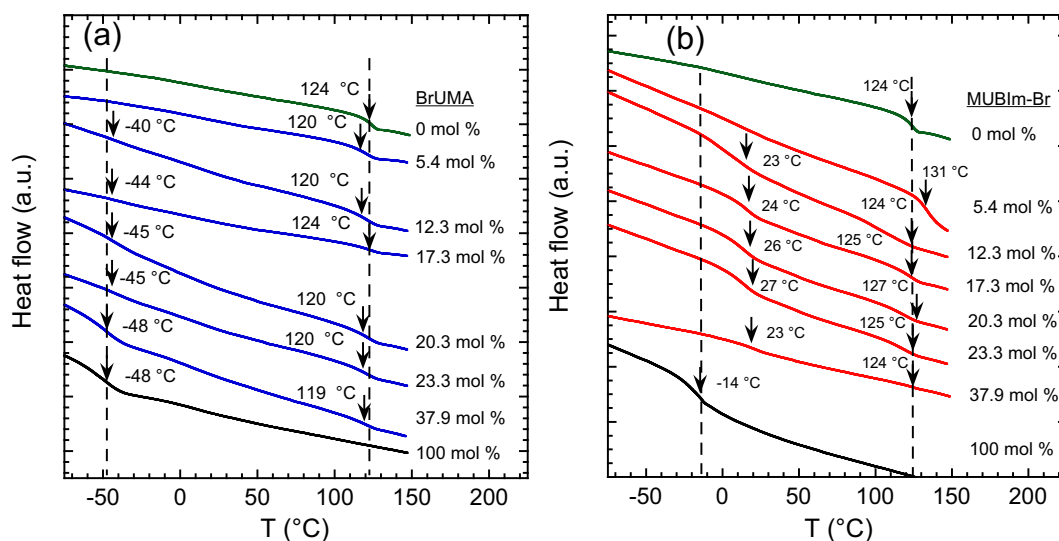


Fig. 3. DSC thermograms of (a) non-ionic precursor PIL block copolymers and (b) ionic PIL block copolymers at various BrUMA and MUBIm-Br compositions, respectively. Homopolymers are also displayed (0 and 100 mol% BrUMA and MUBIm-Br, respectively). Data offset for clarity.

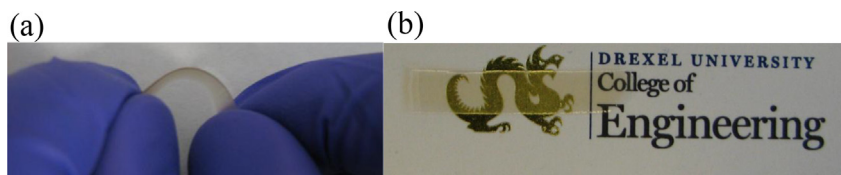


Fig. 4. (a) Flexibility and (b) transparency of a 150 μm film of poly(MMA-*b*-MUBIm-Br-23.3).

12.51 mS cm^{-1} of all polymers and the PIL block copolymer with the highest IEC (1.90 meq/g; 37.9 mol% MUBIm-Br) has the highest conductivity among the PIL block copolymers of 8.67 mS cm^{-1} . Interestingly, at 80 °C and 90% RH, all of the PIL block copolymers (with the exception of lowest composition of 5.4 mol% MUBIm-Br) have higher conductivities compared to the homopolymer. Similar results (higher conductivity in block copolymer compared to its analogous homopolymer) were recently observed for a PIL block copolymer with similar chemistry, but shorter alkyl side-chain length [9]. We hypothesize that water-assisted ion mobility is accelerated in these PIL block copolymers compared to PIL homopolymers due to nanochannel phase-separated domains. It is not clear why these results are temperature dependent in this study, where this was not observed in our previous study [9]. The highest conductivity at 80 °C and 90% RH is 64.85 mS cm^{-1} for the PIL block copolymer at 1.44 meq/g IEC (23.3 mol% MUBIm-Br), while the PIL homopolymer has a conductivity of 21.37 mS cm^{-1} at these similar conditions. Interestingly, the bromide conductivity at these conditions for this PIL block copolymer poly(MMA-*b*-MUBIm-Br) (64.85 mS cm^{-1}) is an order of magnitude higher than the PIL block copolymer poly(MMA-*b*-MEBIm-Br) (5.67 mS cm^{-1}) from our previous study with similar chemistry, similar IEC, higher water content, but shorter alkyl side-chain length [9]. These results

further suggest that water-assisted ion transport is highly morphology dependent. Morphology characterization is not trivial as it is dependent on water content in the polymer and is beyond the scope of this current investigation; an in-depth morphology analysis as a function of humidity is currently underway in our laboratory and will be the subject of a future study.

The impact of water on bromide ion transport is of interest, since a primary transport mechanism in ion-containing polymers is a water-assisted process [17]. Fig. 5b shows the water content in the polymers at high humidity as a function of temperature measured by dynamic vapor sorption. The polymer equilibrium water contents are constant over this temperature range, but increase with increasing IEC from approximately 4–21 wt%, where the highest PIL block copolymer composition is ~ 14 wt% and the PIL homopolymer is ~ 21 wt%. There does not appear to be a clear trend between bromide conductivity of different polymers and absolute water content, specifically since the trends between conductivity and IEC appear to be temperature dependent, while water content appears to be temperature independent. In other words, it is not clear why ion conductivity relatively increases with increasing IEC and water content at 50 °C and 90% RH, but appears to decrease with increasing at 80 °C and 90% RH (Fig. 5c) with the exception of the PIL block copolymer at 5.4 mol% BrUMA composition (0.47 meq/g). This phenomenon is unusual for water-assisted ion transport (e.g., protons, hydroxide, chloride) in ion-containing polymers and therefore suggests other mechanisms impact transport phenomena in PIL block copolymers. Fig. 5d also shows that bromide ion conductivity increases with increasing IEC at a low temperature (~ 23 °C) when saturated in liquid water similar to the results observed at 50 °C and 90% RH.

Although previous work has shown proton transfer in imidazolium-containing polymers, we do not expect proton

Table 3
Mechanical properties of PIL block copolymer poly(MMA-*b*-MUBIm-Br-23.3).

Sample	Tensile strength (MPa)	Young's modulus (GPa)	Elongation at break (%)
Poly(MMA- <i>b</i> -MUBIm-Br-23.3)	12.1 \pm 2.6	0.74 \pm 0.06	3.4 \pm 1.1
Nafion 212	19.3 \pm 2.1	0.22 \pm 0.05	189.0 \pm 7.1

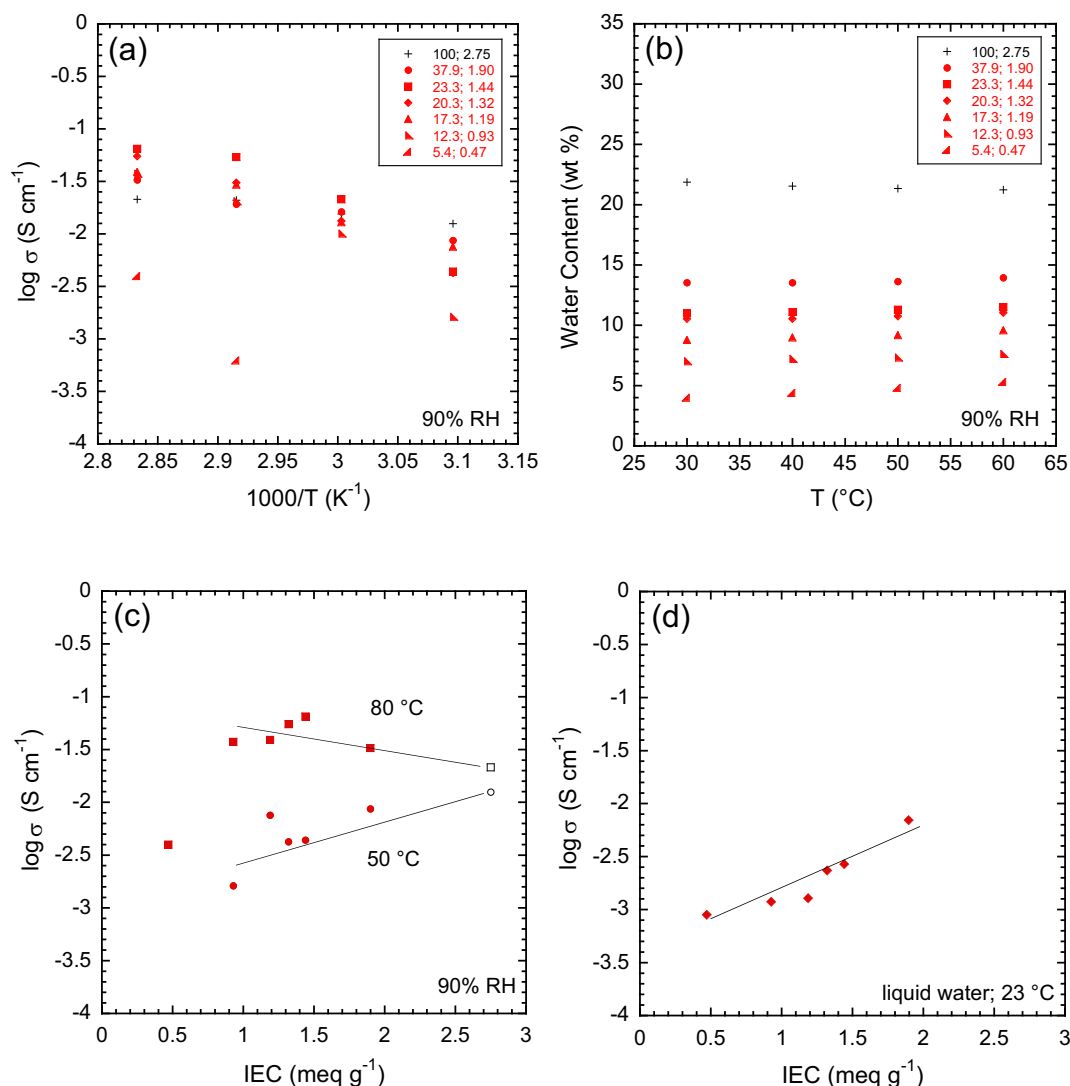


Fig. 5. (a) Bromide ion conductivity and (b) water content as a function of temperature at 90% RH and bromide ion conductivity as a function of IEC at (c) 90% RH at 50 and 80 $^{\circ}C$ and (d) saturated in liquid water at 23 $^{\circ}C$ for the PIL block copolymers poly(MMA-*b*-MUBIm-Br) at various compositions and the PIL homopolymer poly(MUBIm-Br). Numbers in inset legends correspond to MUBIm-Br composition (mol%) and IEC (meq/g) of each polymer. Lines on graphs correspond to trend lines to help guide the eye.

transfer in this imidazolium-bromide chemistry [14,26]. Previous work in our laboratory on the investigation of water in imidazolium-bromide containing polymers using *in situ* FTIR-ATR spectroscopy shows no evidence of protonated water [9]. This suggests that the conductivity measured in this single-ion conductor polymer system is solely due to bromide ions.

4. Conclusions

A series of bromide conducting PIL diblock copolymers, poly(MMA-*b*-MUBIm-Br), with long alkyl side-chain length, were successfully synthesized *via* post-functionalization of the non-ionic precursor block copolymer, poly(MMA-*b*-BrUMA), which was synthesized *via* reversible addition-fragmentation chain transfer (RAFT) polymerization. The PIL block copolymer at 1.44 meq/g (23.3 mol% MUBIm-Br) resulted in flexible, transparent films with high mechanical strength (0.74 GPa modulus) and high bromide ion conductivity (64.85 $mS\ cm^{-1}$ at 80 $^{\circ}C$ and 90% RH). At 80 $^{\circ}C$ and 90% RH, the conductivity of the PIL block copolymer (1.44 meq/g) was three times higher than its analogous PIL homopolymer (2.75 meq/g; 100 mol% MUBIm-Br) and an order of magnitude higher than a

similar PIL block copolymer with shorter alkyl side-chain length. At 50 $^{\circ}C$ and 90% RH, conductivity increases with increasing PIL composition (IEC), but at 80 $^{\circ}C$ and 90% RH, conductivity decreases with increasing IEC. This unusual result warrants further study into the conductivity–morphology relationships in PIL block copolymers, specifically as a function of humidity and temperature, since these are conditions of interest for applications, such as alkaline fuel cells.

Acknowledgments

This work is supported in part by the U.S. Army Research Office under grant no. W911NF-07-1-0452 Ionic Liquids in Electro-Active Devices (ILEAD) MURI and the Nanotechnology Institute under grant no. NTI 1001-037.

References

- [1] Weber RL, Ye Y, Schmitt AL, Banik SM, Elabd YA, Mahanthappa MK. *Macromolecules* 2011;44:5727–35.
- [2] Ye Y, Choi JH, Elabd YA, Winey KI. *Macromolecules* 2012;45:7027–35.
- [3] Choi JH, Ye Y, Elabd YA, Winey KI. *Macromolecules* 2013;46:5290–300.

- [4] Green MD, Choi JH, Winey KI, Long TE. *Macromolecules* 2012;45:4749–57.
- [5] Cheng S, Beyer FL, Mather BD, Moore RB, Long TE. *Macromolecules* 2011;44:6509–17.
- [6] Gu Y, Lodge TP. *Macromolecules* 2011;44:1732–6.
- [7] Nguyen PT, Wiesenauer EF, Gin DL, Noble RD. *J Memb Sci* 2013;430:312–20.
- [8] Green MD, Wang D, Hemp ST, Choi JH, Winey KI, Heflin JR, et al. *Polymer* 2012;53:3677–86.
- [9] Ye Y, Sharick S, Davis EM, Winey KI, Elabd YA. *ACS Macro Lett* 2013;2:575–80.
- [10] Wanakule NS, Virgili JM, Teran AA, Wang ZG, Balsara NP. *Macromolecules* 2010;43:8282–9.
- [11] Young WS, Epps TH. *Macromolecules* 2012;45:4689–97.
- [12] Soo PP, Huang BY, Jang YI, Chiang YM, Sadoway DR, Mayes AM. *J Electrochem Soc* 1999;146:32–7.
- [13] Simone PM, Lodge TP. *ACS Appl Mater Interfaces* 2009;1:2812–20.
- [14] Hoarfrost ML, Tyagi MS, Segalman RA, Reimer JA. *Macromolecules* 2012;45:3112–20.
- [15] Gwee L, Choi JH, Winey KI, Elabd YA. *Polymer* 2010;51:5516–24.
- [16] Ye Y, Elabd YA. *Polymer* 2011;52:1309–17.
- [17] Ye Y, Elabd YA. *Macromolecules* 2011;44:8494–503.
- [18] Elabd YA, Hickner MA. *Macromolecules* 2011;44:1–11.
- [19] Tanaka M, Fukasawa K, Nishino E, Yamaguchi S, Yamada K, Tanaka H, et al. *J Am Chem Soc* 2011;133:10646–54.
- [20] Tsai TH, Maes AM, Vandiver MA, Versek C, Seifert S, Touminen M, et al. *J Polym Sci Polym Phys* 2013;51:1751–60.
- [21] Rebeck NT, Li Y, Knauss DM. *J Polym Sci Polym Phys* 2013;51:1770–8.
- [22] Yu S, Yan F, Zhang X, You J, Wu P, Lu J, et al. *Macromolecules* 2008;41:3389–92.
- [23] Weiss RA, Fitzgerald JJ, Kim D. *Macromolecules* 1991;24:1071–6.
- [24] Dai H, Zhang H, Luo Q, Zhang Y, Bi C. *J Power Sources* 2008;185:19–25.
- [25] Ishiyama C, Higo Y. *J Polym Sci Polym Phys* 2002;40:460–5.
- [26] Xiao L, Zhang H, Scanlon E, Ramanathan LS, Choe E-W, Rogers D, et al. *Chem Mater* 2005;17:5328–33.